ROMANIAN JOURNAL OF INFORMATION SCIENCE AND TECHNOLOGY
Volume **26**, Number 2, 2023, 205–217

Relationship Between Structural and Optical Properties in Vanadium Pentoxide

Cosmin ROMANITAN[1], Iuliana MIHALACHE[1], Silviu VULPE[1], Marius STOIAN[1], Ioan-Valentin TUDOSE[2,3], Raluca GAVRILA[1], Pericle VARASTEANU[1], Marian POPESCU[4], Oana BRINCOVEANU[1], Nikolay DJOURELOV[5], Emmanouel KOUDOUMAS[2], and Mirela SUCHEA[1,2,*]

[1]National Institute for Research and Development in Microtechnologies -IMT-Bucharest, 126A Erou Iancu Nicolae Street, Voluntari 077190, Romania

[2]Center of Materials Technology and Photonics and School of Engineering, Hellenic Mediterranean University, 71410 Heraklion, Crete, Greece

[3]Chemistry Department, University of Crete, 70013 Heraklion, Greece

[4]Chemistry Department, University of Crete, 70013 Heraklion, Greece

[4]Extreme Light Infrastructure-Nuclear Physics (ELI-NP), *Horia Hulubei* National R&D Institute for Physics and Nuclear Engineering (IFIN-HH), Magurele, Ilfov 077125, Romania

E-mails: cosmin.romanitan@imt.ro; iuliana.mihalache@imt.ro; silviu.vulpe@imt.ro; marius.stoian@imt.ro; tudose_valentin@yahoo.com; raluca.gavrila@imt.ro; pericle.varasteanu@imt.ro; fluidproject@gmail.com; oana.brincoveanu@imt.ro; nikolay.djourelov@eli-np.ro; koudoumas@hmu.gr; mirasuchea@hmu.gr*

* Corresponding author

Abstract. *Spray pyrolysis technique* (SPT) and *radio-frequency magnetron sputtering* (RF-MS) were used to obtain *vanadium oxide* (V_xO_y) layers. The surface morphology was visualized using *scanning electron microscopy* (SEM) and *atomic force microscopy* (AFM). Further, the microstructure was assessed by means of *X-ray diffraction* (XRD), showing the formation of *orthorhombic* V_2O_5 ($\alpha - V_2O_5$) with high crystallinity by SPT. On the other side, RF-MS at low substrate temperature led to $\alpha - V_2O_5$ with low crystallinity, even at 800 swipes which according to the Kiessig interference fringes from X-ray reflectivity indicates a film thickness of 70 nm. Finally, *diffuse reflectance spectroscopy* (DRS) absorbance was used to investigate the optical properties for the obtained samples, noting important differences regarding the bandgap energy between SPT and RF-MS depositions. To explain the observed discrepancies, *X-ray photoelectron spectroscopy* (XPS) was performed, thus obtaining a correlation of the bandgap to the oxidation state of vanadium ions.

Key-words: RF magnetron sputtering; spray pyrolysis technique; vanadium oxide; X-ray diffraction.

1. Introduction and Preliminary Results

Vanadium oxides compounds have received a constantly growing interest in materials science, due to their ability to tune the material properties according to the oxidation state (V^{2+}, V^{3+}, V^{4+}, and V^{5+}) [1, 2] and the conducted studies revealed a plethora of applications derived from vanadium oxide materials. For instance, thin films of VO_2 and V_2O_3 have been found to show good thermochromism in the infrared region and moreover, the metal-insulator transition (MIT) with the change in temperature is related to thermo and electrochromic applications, such as smart windows [3], ultra-fast nanoelectronic switches [4] transistors [5], thermoelectric devices [6]. Vanadium pentoxide (V_2O_5) is the most stable compound and has attracted much attention owing to its unique electronic, chemical, and optical properties, arousing interest in the broadband photodetectors [7], gas sensors [8, 9] and electrochromic devices [10–12].

The structural properties of V_2O_5 play a critical role in determining its optical properties, such as its absorption, reflectance, and transmission spectra. One important structural property of V_2O_5 is its crystal structure, which can be varied depending on the synthesis method and processing conditions. For example, V_2O_5 can exist in several different crystal structures, including orthorhombic, monoclinic, and amorphous phases, each with different optical properties [13]. Among these, the orthorhombic phase of V_2O_5 ($\alpha - V_2O_5$) has been shown to have a high degree of crystallinity and exhibits strong absorption in the ultraviolet and visible regions of the electromagnetic spectrum, which makes it suitable for use as a UV-blocking material in coatings and sunscreens. Another important structural property of V_2O_5 is its morphology, which also affects its optical properties. For instance, V_2O_5 nanostructures have been shown to exhibit enhanced optical properties compared to their bulk counterparts, due to their high surface area and increased light scattering and absorption. In addition, one-dimensional structures have been shown to exhibit strong near-infrared absorption, which makes them attractive for use in energy storage and photovoltaic devices [14]. The optical properties of V_2O_5 can also be influenced by doping with other elements, which can alter the electronic structure and bandgap of the material. For example, the optical properties of V_2O_5 can be tuned by introducing W or Mo dopants, which can shift the absorption spectra to longer wavelengths and improve the material's charge transport properties [15, 16]. Therefore, the structural properties of V_2O_5, such as its crystal structure, morphology, and doping, are closely related to its optical properties and can be tailored for specific applications in optical devices, energy storage, and catalysis. Furthermore, it was suggested that the regular stacking of the atomic planes along (001) in crystalline V_2O_5 is very favorable for the intercalation of hosts for Li ions, like in rechargeable batteries [17, 18] since such a well-aligned structure would enhance the Li^+ diffusion through the solvent. Moreover, amorphous V_xO_y became popular for Li- and Na-ion batteries [19], high-energy Li-ion anodes [20], or positive electrode in rechargeable aluminum battery [21].

Whereas crystalline vanadium oxide thin films can be obtained by RF-magnetron sputtering or pulsed laser deposition at elevated substrate temperatures [22], amorphous vanadium oxide thin films can be obtained by electrochemical oxidation [23], reactive sputtering [24], using a combination of sol-gel processing paired with electrochemical deposition [25], atomic layer chemical vapor deposition [19], atomic layer deposition [26], or gas impulse magnetron sputter-

ing [21]. In order to have VO_x layers with high specific surface area, different methods were proposed to obtain vanadium oxide in nanostructured form, such as electrospinning of V_2O_5 nanofibers, electrostatic spray-deposition, deposition of V_2O_5 nanowires from chemical vapor transport or spray pyrolysis technique [27].

One of the most important parameters for assesing the properties of materials is the bandgap energy (Eg), which is affected by the crystallographic structure, stoichiometry, internal strain, crystal quality or dimensionality (*i.e.* thin film/nanostructured) or oxidation state [1]. The electronic structure of V_2O_5 has been the subject of intensive studies and various theoretical calculations of band structure that include both semiempirical and ab initio techniques [28–30] and it was found a large variation in the visible region [1, 31].

This paper represent an extension of our recent published paper [32], in which we presented the preparation methods and some preliminary characterization of vanadium oxide layers, without to explain different observed bandgaps values. Herein, the morpho-structural properties of V_2O_5 samples obtained by *spray pyrolysis technique* (SPT) and *radio-frequency magnetron sputtering* (RF-MS) in correlation with their optical properties are presented. The crystal structure was resolved by *X-ray diffraction* (XRD) by Rietveld refinement, while the band gap energy was evaluated by *diffuse reflectance spectroscopy* (DRS) and *Kubelka-Munk* (K-M) transformation. An explanation of the relative high value of the band gap energy for the samples obtained by RF-MS was provided considering the presence of V^{4+} oxidation state, as proved by *X-ray photoelectron spectroscopy* (XPS) investigations.

The next section presents the experimental details for the SPT and RF-MS, as well as the characterization tools. Then, Section 3 is dedicated to the application of different characterization tools, as follows: scanning electron and atomic force microscopy (SEM/AFM), XRD/XRR, DRS and XPS to investigate the sample microstructure and the optical properties. Section 4 concludes this paper.

2. Experimental Details

During the SPT deposition, a custom-made spray pyrolysis setup was used, and more details can be found in previously reported work of the same group [33]. *Fluoride tin oxide* (FTO) coated glass substrates were used for deposition, keeping a temperature of 250 °C, employing different quantities and concentrations for the precursor: (5mL_0.01M); (10mL_0.01M); (5mL_0.02M); (10mL_0.02M). After deposition, the samples were subjected to a thermal treatment of 400 °C, following the procedures described in [34]. In the RF-MS deposition case, silicon (Si) substrates were used at constant growth parameters (Ar:N = 20:1 in sscm, power RF = 300 W, deposition temperature = 60 °C, chamber pressure = 5 mTorr, power = 300 W), while the number of the swipes was varied from 100 up to 800 swipes.

Grazing incidence XRD investigations were performed using a 9 kW Rigaku SmartLab diffractometer in 2θ mode, keeping the incidence angle at 0.5 °. *X-ray reflectivity* (XRR) spectra were recorded in $\theta/2\theta$ mode in a medium resolution configuration with open detector. *Scanning electron microscopy* (SEM) characterization was performed using a field emission scanning electron microscope Nova NanoSEM 630 (FEI Company, Hillsborough, OR, USA). The AFM micrographs have been acquired using Ntegra Aura (Nt-MDT) equipment, operated in semicontact (intermittent-contact) mode. *Diffuse reflectance spectroscopy* (DRS) was performed using an integrating sphere placed inside a FLS920 spectrometer (Edin. Inst. Ltd, UK) equipped with 450 W Xe lamp and the excitation light was dispersed by a monochromator with 1800 grooves/mm

grating (0.1 nm resolution). *X-ray photoemission spectroscopy* (XPS) spectra were recorded on a Sigma Surface Science photoelectron spectrometer equipped with a 160-mm hemispherical energy analyzer with a 1D detector (ASPECT) and using an Al K_α X-ray source at 13 kV at a power of 200 W. All spectra were fitted using a Shirley type background and a Lorentzian-Gaussian peak shape.

3. Results and Discussion

3.1. Scanning electron and atomic force microscopy characterization

To study the surface morphology of the obtained samples by SPT, top-view SEM micrographs were recorded according to Fig. 1 (a).

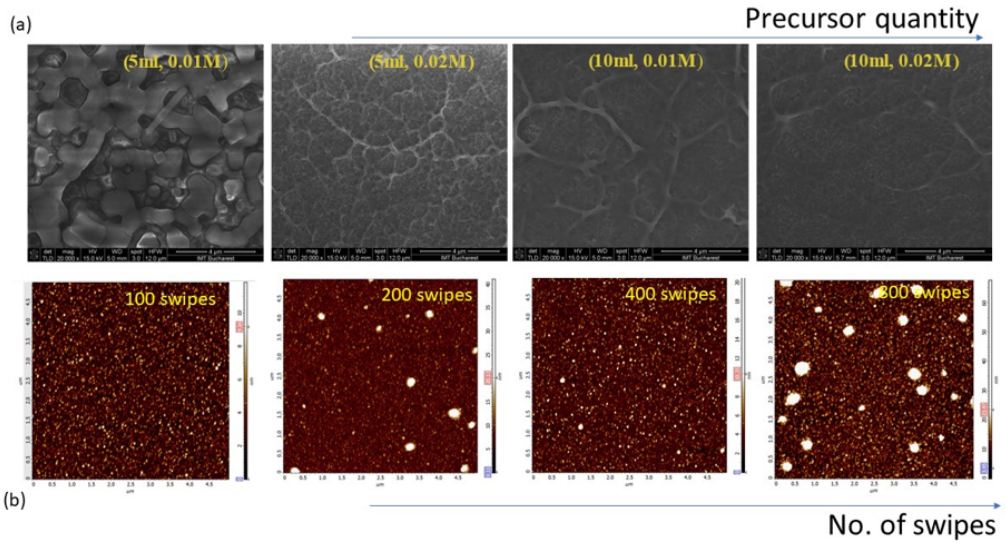

Fig. 1. (a) Top-view SEM micrographs for the obtained samples by SPT, by varying the solution concentration and its volume (values are listed above). (b) AFM images of the samples achieved by RF-MS at 100, 200, 400 and 800 swipes (scan size: 5 μm).

The SEM micrographs show the presence of the large grains when a low precursor quantity was used, while for larger precursor quantity the surface morphology consists of a combination of irregular walls with high aspect ratio and granular nanostructured flat film regions. The walls width is below 1 μm, while the length reaches up to 10 μm. In previous studies of surface morphology for vanadium oxide obtained by SPT, it was observed a close dependence of width of the walls on the deposition conditions, as reported in [33]. More specifically, it was found that the width increased with the precursor quantity from 300 to 800 nm, and correlate also with a better crystallization at higher precursor quantity. Overall, the samples obtained through RF-MS exhibit a smooth surface composed of fine and uniform grains, even after 800 cycles (see Fig. 1b). However, as the number of cycles increases and the films are becoming thicker, the surface tends to develop additional globular agglomerations that grow in size and density. The results

presented in the next section suggest that the different crystal quality could be responsible for the different surface morphology features observed by microscopic techniques.

3.2. X-ray diffraction and reflectivity

Accordingly, the microstructure of each sample was investigated by grazing incidence X-ray diffraction as shown in Fig. 2 (a).

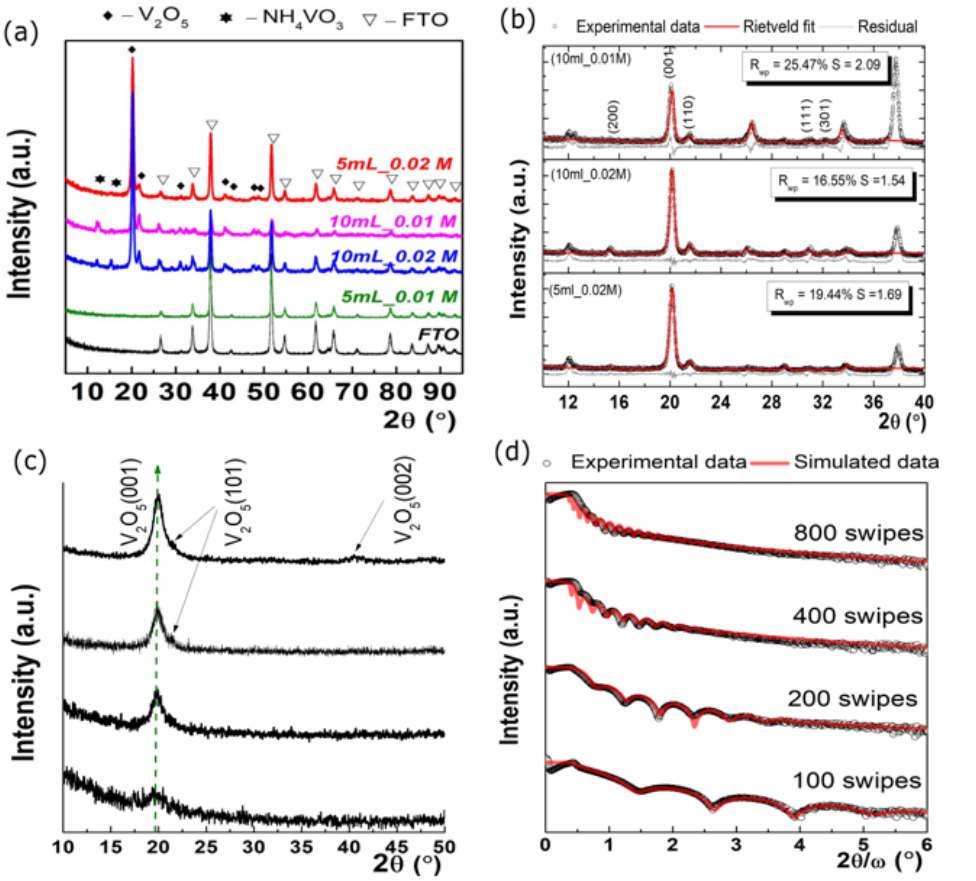

Fig. 2. (a) Grazing incidence XRD patterns for the investigated samples and FTO substrate. The identification of the diffraction peaks was made using ICDD database, thus: $\alpha - V_2O_5$ (diamond symbol), NH_4VO_3 (star) and FTO substrate (star). (b) Experimental data (black points) and Rietveld fit (red line), as well as the difference between the experimental and calculated data (grey line). In the inset are presented the fitting parameters, R_{wp} and S. (c) Experimental XRR data (points) with the simulated data (line) and (d) GI-XRD patterns for RF-MS samples.

One can observe that the X-ray diffraction patterns present a large number of diffraction peaks. Most of them are attributed to FTO substrate (black line) and other diffraction peaks located at 20.35°, 21.59°, 32.10°, 33.75°, 42.00°, 47.71° and 48.84° are unambiguously as-

signed as (001), (101), (011), (111), (002), (600) and (021) reflections of $\alpha - V_2O_5$ phase with $a = 1.148$ nm, $b = 0.436$ nm, and $c = 0.355$ nm, that belongs to 47:Pmmm space group with orthorhombic symmetry (diamond symbol). Moreover, the unreacted metavanadate compounds from the synthesis processes are also detected by XRD at 10 mL. It seems that in the case of 5 mL at 0.01 M concentration the film was not yet formed at low precursor concentration (green line). As recently reported in [35], the strong intensity of (001) reflection at 20.35° suggests a regular stacking of imperfect ab planes built up of vanadyl oxygen and that the c-axis is perpendicular to the surface sample [36]. In our recent work, we have shown that the texture coefficient (i.e. preferential orientation) along (001) reflection is closely related to the inserted charge density in $\alpha - V_2O_5$, key parameter for the electrochromic and charge storage devices [33]. Obviously, the different synthesis parameters influence the formation and the crystal quality of V_2O_5 films, as well as the texture coefficient. An assessment of the microstructural features was made using Rietveld refinement method. In this framework, the pattern fitting is performed over a broad angular range, based on reasonable initial approximation of unit cell dimensions or coordinates of all atoms in crystal. The theoretical profile, y_i^{calc}, has the following expression [37]:

$$y_i^{calc} = A(2\theta) \sum_n s_n \sum_h P_{n,h} I_{n,h} \phi_n (2\theta_i - 2\theta_h - T(2\theta_i)) + y_b(2\theta_i) \quad (1)$$

Here, s_n is the scale factor, $2\theta_h$ the Bragg angle, A(2θ) the absorption and irradiation correction, $P_{n,h}$ the preferred orientation correction, $I_{n,h}$ the integrated intensity function, T($2\theta_i$) the angular correction, and y_b ($2\theta_i$) the background function. During the Rietveld refinement, multiple features of the patterns were considered. For instance, the background was modeled with a B-spline function, the peak shift with the shift axial displacement model, the peak shapes using pseudo-Voigt fits, while the preferred orientation with the March-Dollase function. The fitting of the theoretical profile, y_i^{calc},was performed over the experimental data using a least-squared minimizing procedure and a set of numerical figures of merit (FOM's): reliability factor (R_p), the weighted parameter (R_{wp}), the scale factor (S), the expected profile residual, R_e and the goodness of the fit, χ^2.

In Fig. 2 (b), the red line depicts the Rietveld data with the corresponding R_{wp} and S fitting, which indicate the fitting accuracy of the refinement. The values of the mean crystallite size, the unit cell parameters and the average lattice strain are presented in Table 1. The results indicate that the unit cell parameters are not affected by either solution quantity or molarity. However, a smaller mean crystallite size, accompanied by a higher lattice strain, was found at the concentration 5 mL with 0.02 M molarity. Further, when the molarity increased, the mean crystallite size also increased, and at the same time, the lattice strain became smaller.

Table 1. Unit cell parameters, mean crystallite size and the lattice strain

Sample	a, b, c (nm)	τ (nm)	ε (%)
5ml_0.01M No crystalline film formed	–	–	–
5ml_0.02M	1.18, 0.34, 0.43	17.8	0.26
10ml_0.01M	1.18, 0.34, 0.43	19.6	0.21
10ml_0.02M	1.18, 0.34, 0.43	18.7	0.15

In the case of RF-MS samples, XRR and XRD curves were used to investigate how the number of swipes affects the layer's thickness and crystal quality, when the swipe number increased from 100 to 200, then to 400, reaching to 800 according to Fig. 2 (c) and (d).

In each case, the reflectivity profiles present periodic fringes that stem from the interference at the boundary at the layer and substrate and are called Kiessig fringes. Their period, $\Delta\theta$ in radians is related to the layers thickness, τ through the following relation [38]:

$$\tau = \frac{\lambda}{\Delta\theta} \tag{2}$$

where λ is the X-ray wavelength (0.154 nm).

According to the period of interference fringes, the thickness increases from 7 to 70 nm when the number of the swipes is modified from 100 to 800. The thickness of each sample is illustrated in Table 2.

Table 2. Number of swipes, thickness calculated from XRR and the mean crystallite size determined from the Rietveld refinement

Swipes	Thickness (nm)	Mean crystallite size (nm)
100	6.8	–
200	15.9	5.8
400	32.5	6.4
800	70.1	7.1

Concomitantly, GI-XRD data indicate the formation of the (001) $\alpha - V_2O_5$ and the diffraction peak becomes narrower at higher thickness, since the crystalline domains become also higher, as it will be shown by Scherrer's equation. This further implies the emergence of (101) and (002) reflections at higher thickness. The Scherrer's equation gives the relationship between the size of the crystalline domains, τ in respect to the peak broadening, and β expressed in radians in the following way:

$$\tau = \frac{k\lambda}{\beta cos\theta} \tag{3}$$

where k is the shape factor, taken equal to 0.93 in this study, λ is the X-ray wavelength and θ is the angular position of the (100) diffraction peak. According to Scherrer's equation, there is a variation of the mean crystallite size from amorphous domains to crystalline domains with size of 7 nm (*e.g.* 800 swipes). The values of the crystalline domains size are tabulated in Table 2. That indicates that, at the low temperature of the substrate (~ 60°C), the deposited material may be just sticking to the Si/SiO_2 substrate surface, with almost no surface diffusion [22]. The substrate temperature is not high enough to provide sufficient thermal energy to the ad-atoms to find the locations for further bonding, resulting in structure with poor crystal quality. On the other hand, sharp diffraction peaks were found in SPT deposition, for which the samples were obtained at a substrate temperature of 250 °C, further subjected to a thermal treatment at 400 °C in O_2 atmosphere. Previous XRD studies showed that the deposition of crystalline V_2O_5 phase occurs at around 200 °C in the case of d.c. reactive magnetron sputtering [39].

3.3. Optical measurements

In order to establish the influence of the microstructure in the optical properties, the *diffuse reflectance spectroscopy* (DRS) and *Kubelka-Munk* (K-M) transformation were employed, to estimate the optical band gap in SPT deposition shown in Fig. 3 (a).

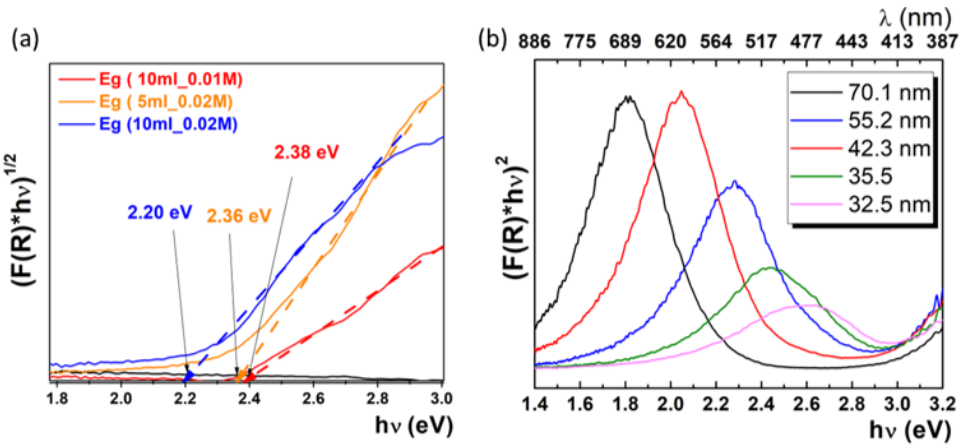

Fig. 3. Diffuse reflectance spectra for the investigated samples obtained by (a) SPT and (b) RF-MS.

For this purpose, it is necessary to evaluate correctly the interband transition in the investigated samples, namely direct, indirect or both. The available literature on the bandgap of V_2O_5 is vast and shows that the bandgap is affected by thin film deposition technique, thickness, substrate type or non-stoichiometry [1]. In most cases, it was found that a direct allowed transition is the most probable one in $\alpha - V_2O_5$. However, transmission measurements conducted by [40] for sputtered $\alpha - V_2O_5$ indicated two distinct interband transitions, implying direct and indirect transition. In particular, since $\alpha - V_2O_5$ obtained by SPT is crystalline, a direct interband transition was considered in Kubelka-Munk transformation. On the other hand, considering the low crystallinity of VO_x in the case of RF-MS samples and the presence of V^{4+} ions in these samples (as it will be proved by XPS), the interband transition was considered rather indirect. According to the calculations, the band gap falls within the range 2.20 eV – 2.40 eV, which is a typical range for vanadium pentoxide deposited using SPT [41], suggesting the presence of pure $\alpha - V_2O_5$. Studies have reported the bandgap of V_2O_5 films synthesized by spray pyrolysis to be in the range of 2.2-2.6 eV [42–44]. Mousavi *et al.* [45] observed that for V_2O_5 films prepared by spray pyrolysis Eg changes with the substrate temperature (T_{sub}), considering also a direct interband transition. When T_{sub} increases, the E_g decreases gradually from 2.46 to 2.22 eV, due to the modification of the extinction coefficient at different temperatures. The authors reported that the optical bandgap of the V_2O_5 films ranged from 2.4 to 2.6 eV, depending on the deposition parameters. In the present study case, the substrate temperature was kept constant, and the modifications could be explained by taking into account different synthesis parameters. More specifically, one can observe that the band gap of the material reported here is quite low and decreases from 2.38 eV to 2.36 eV and then to 2.20 eV when the precursor quantity is high. This can be associated to the higher thickness and improved crystallinity. On the other hand, the RF-MS samples present two regions. At high wavelength, it can be observed an absorption peak given by Si ($E_g = 1.1$ eV), while V_2O_5 layer absorbs at lower wavelength. It should be mentioned that the samples obtained at 100 and 200 swipes could not be analyzed, due to their small thickness, *i.e.* 6.8 nm and 15.9 nm, respectively. In this case, we chose the thicker V_2O_5 samples. Fig. 3 (a) gives the evolution of the absorption spectra with V_2O_5 thickness. Whereas the band

gap of the SPT samples was found in the range of 2.2 and 2.4 eV, in the case of RF-MS the band gap is significantly wider, with values ranging from 2.82 eV to 2.90 eV at 70.1 nm. Studies that have reported optical bandgap values for RF sputtered V_2O_5 films on Si reported bandgaps values ranging from 2.5 to 3.3 eV [46–48]. The origin of the UV absorption was extensively studied by Meyn *et al.* [49], who reported that the UV light absorption in the oxides can be enhanced by tetravalent vanadium ion V^{4+} presence. Thus, it is considered that the PL properties of vanadium oxide thin films strongly depend on the oxidation state. Furthermore, relative high values for band gap in RF-MS can be explained considering the low substrate temperature during the sample deposition. Kang *et al.* [40] showed that the interband transition is dependent on the substrate temperature during deposition, and the bandgap decreases as the substrate temperature increases in RF-MS deposition. To explain the higher band gap energy at high thickness for the RF-MS sputtered films, it was studied the dependence of the oxidation state with the thickness by XPS.

3.4. XPS

XPS investigation was carried out on V_2O_5 2 /Si samples, to obtain information related to the oxidation state of vanadium ions. Fig. 4 shows the XPS spectra recorded at 100, 200, 400 and 800 swipes.

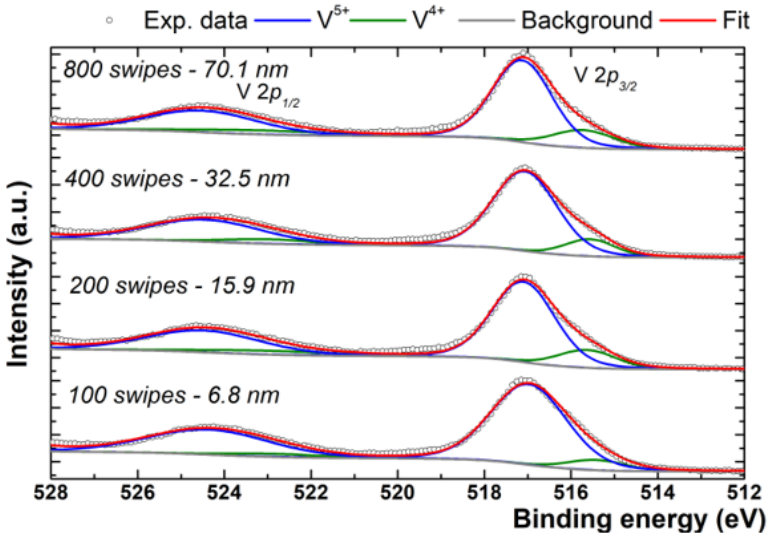

Fig. 4. Experimental XPS spectra for the obtained samples by RF-MS at 100, 200, 400, 800 swipes (black points) and the corresponding fits.

It is revealed the presence of V $2p$ doublet and the fitting were performed using a mixed LorentzianGaussian function. Due to spin splitting, the V $2p_{3/2}$ and V $2p_{1/2}$ signal areas have a fixed 2:1 ratio and fixed shift of 7.4 eV. The V_2O_5 presence is proved by given by the spin-orbit splitting of approximately 7.5 eV between V $2p_{3/2}$ and V $2p_{1/2}$ orbitals [25], [50]. The V $2p_{3/2}$ and V $2p_{1/2}$ were deconvoluted using V^{4+} (binding energy, $BE = 515.5$ and 523 eV) and V^{5+} ($BE = 517.1$ and 524.7 eV) oxidation states. The binding energy values for vanadium oxides

are in a good agreement with the previous work on vanadium pentoxide [51, 52]. The integral areas provided by the deconvolution procedure normalized at the atomic sensitivity factors were used to determine the distribution between the V^{4+} and V^{5+} states in the V 2p signal [53]. Thus, it was shown that the oxidation state depends by the layer thickness. Whereas in the thinnest sample has the smallest V^{4+} content, $V^{4+}(\%)$ = 8.9%, in the case of the thickest one, $V^{4+}(\%)$ becomes 18.5%. A higher V^{4+} content in the thick sample could be responsible for the observed band gap in this sample (*e.g.* 2.9 eV), while the other samples have the band gap around of 2.83 eV. Overall, it is suggested the close relationship between the oxidation state and the observed band gap in V_2O_5.

4. Conclusions

Spray pyrolysis technique, SPT, and radio-frequency magnetron sputtering, RF-MS, were used to obtain vanadium oxide, V_xO_y, thin films. The surface morphology was visualized using scanning electron microscopy, SEM, and atomic force microscopy, AFM. Further, the microstructure was assessed by means of X-ray diffraction, XRD, showing the formation of orthorhombic V_2O_5 ($\alpha - V_2O_5$) with high crystallinity for films made by SPT. On the other side, RF-MS at low substrate temperature led to $\alpha - V_2O_5$ with low crystallinity, even at 800 swipes (*i.e.* 70 nm thickness estimated according to the Kiessig interference fringes from X-ray reflectivity). Finally, diffuse reflectance spectroscopy, DRS, absorbance were used to investigate the optical properties for the obtained samples, noting important differences regarding the bandgap energy between SPT and RF-MS deposition. In the case of SPT deposited thin films, low optical band gap values from 2.2 to 2.4 eV were obtained whole for the RF-MS films the optical bandgap values were higher ranging from 2.82 eV to 2.90 eV at 70.1 nm. To explain the observed differences, X-ray photoelectron spectroscopy, XPS, was performed, thus obtaining a correlation of the bandgap to the oxidation state of vanadium ions.

Acknowledgements. This research was partially financed by Romanian Core Program PNCDI 2022-2027, "Cercetări avansate în dispozitive micro-nano-electronice, fotonice, senzori şi microsisteme pentru aplicaţii societale- μNanoEl" cod 2307/29.12.2022 (2023-2026); financed by the Ministry of Research, Innovation and Digitalization. and MicroNEx, Contract nr. 20 PFE from 30.12.2021 (2022-2024), financed by the Ministry of Research, Innovation and Digitalization through Program 1–Development of the National R & D System, Subprogram 1.2–Institutional Performance–Projects for Institutional Excellence. Also, N.D. acknowledges the support by the contract PN 23.21.01.06 sponsored by the Romanian Ministry of Research, Innovation and Digitalization.

References

[1] K. SCHNEIDER, *Optical properties and electronic structure of V_2O_5, V2O3 and VO2*, Journal of Materials Scence: Materials in Electronics **31**, pp. 10478–10488, 2020.

[2] E. KIANFAR, *Recent advances in synthesis, properties, and applications of vanadium oxide nanotube*, Microchemical Journal **145**, pp. 966–978, 2019.

[3] A.S. MCLEOD, E. VAN HEUMEN, J. G. RAMIREZ, S. WANG, T. SAERBECK, S. GUENON, M. GOLDFLAM, L. ANDEREGG, P. KELLY, A. MUELLER, M. K. LIU, I. K. SCHULLER and D. N.

BASOV, *Nanotextured phase coexistence in the correlated insulator V_2O_3*, Nature Physics **13**, pp. 80–86, 2017.

[4] S. LUPI, L. BALDASSARRE, B. MANSART, A. PERUCCHI, A. BARINOV, P. DUDIN, E. PAPALAZAROU, F. RODOLAKIS, J. P. RUEFF, J. P. ITI, S. RAVY, D. NICOLETTI, P. POSTORINO, P. HANSMANN, N. PARRAGH, A. TOSCHI, T. SAHA-DASGUPTA, O. K. ANDERSEN, G. SANGIOVANNI, K. HELD and M. MARSI, A microscopic view on the Mott transition in chromium-doped V2O3, Nature Communications **1**, pp.105, 2010.

[5] J. JEONG, N. AETUKURI, T. GRAF, T. D. SCHLADT, M. G. SAMANT and S. S. P. PARKIN, *Suppression of metal-insulator transition in VO2 by electric field-induced oxygen vacancy formation*, Science **339**, pp. 1402–1405, 2013.

[6] S. CHEN, Z. WANG, H. REN, Y. CHEN, W. YAN, C. WANG, B. LI, J. JIANG and C. ZOU, *Gate-controlled VO2 phase transition for high-performance smart windows*, Science Advances **5**(3), pp. 1–9, 2019.

[7] H. S. KIM, K. R. CHAUHAN, J. KIM and E. H. CHOI, *Flexible vanadium oxide film for broadband transparent photodetector*, Applied Physics Letters **110**, pp. 101907, 2017.

[8] K. SCHNEIDER, M. LUBECKA and A. CZAPLA, V_2O_5 thin films for gas sensor applications, Sensors Actuators B: Chemical **236**, pp. 970–977, 2016.

[9] M. MAZUR, A. LUBAŃSKA, J. DOMARADZKI and D. WOJCIESZAK, *Complex Research on Amorphous Vanadium Oxide Thin Films Deposited by Gas Impulse Magnetron Sputtering*, Applied Sciences **12**, pp. 8966, 2022.

[10] N. A. CHERNOVA, M. ROPPOLO, C. DILLON and M. S. WHITTINGHAM, *Layered vanadium and molybdenum oxides: batteries and electrochromics*, Journal of Materials Chemistry **19**, pp. 2526–2552, 2009.

[11] K. TAKAHASHI, Y. WANG, G. CAO, K. TAKAHASHI, Y. WANG and G. CAO, *Growth and electrochromic properties of single-crystal V_2O_5 nanorod arrays*, Applied Physics Letters **86**, pp 053102, 2005.

[12] Z. TONG, H. LV, X. ZHANG, H. YANG, Y. TIAN and N. LI, *Novel morphology changes from 3D ordered macroporous structure to V_2O_5 nanofiber grassland and its application in electrochromism*, Scientific Reports **5**, pp. 16864, 2015.

[13] P. GUO, Z. BIEGLER, T. BACK and A. SARANGAN, *Vanadium dioxide phase change thin films produced by thermal oxidation of metallic vanadium*, Thin Solid Films **707**, pp. 138117, 2020.

[14] T. K. LE, M. KANG and S. W. KIM, *A review on the optical characterization of V_2O_5 micro-nanostructures*, Ceramics International **45**, pp. 15781–15798, 2019.

[15] M. PANAGOPOULOU, D. VERNARDOU, E. KOUDOUMAS, D. TSOUKALAS and Y. S. RAPTIS, *Tungsten doping effect on V_2O_5 thin film electrochromic performance*, Electrochimica Acta **321**, pp. 134743, 2019.

[16] M. NAZEMIYAN and Y. S. JALILI, *Record low temperature Mo doped V_2O_5 thermochromic thin films for optoelectronic applications*, AIP Advances **3**, pp. 122103, 2013.

[17] B. B. LAKSHMI, C. J. PATRISSI and C. R. MARTIN, *Sol - gel template synthesis of semiconductor oxide micro- and nanostructures*, Chemistry Materials **20**, pp. 2544–2550, 1997.

[18] B. PANDIT, D. P. DU, P. GÓMEZ-ROMERO, B. B. KALE and B. R. SANKAPAL, *V_2O_5 encapsulated MWCNTs in 2D surface architecture: Complete solid-state bendable highly stabilized energy efficient supercapacitor device*, Scientific Reports **7**, pp. 43430, 2017.

[19] S. PETNIKOTA, R. CHUA, Y. ZHOU, E. EDISON and M. SRINIVASAN, *Amorphous vanadium oxide thin films as stable performing cathodes of lithium and sodium-ion batteries*, Nanoscale Research Letters **13**, pp. 1–13, 2018.

[20] Y. SUN, Z. XIE and Y. LI, *Enhanced lithium storage performance of V_2O_5*, RSC Advanced **8**, pp. 39371–39376, 2018.

[21] M. CHIKU, H. TAKEDA, S. MATSUMURA, E. HIGUCHI and H. INOUE, *Amorphous Vanadium oxide/carbon composite positive electrode for rechargeable aluminum battery*, ACS Applied Materials & Interfaces **7**, pp. 24385–24389, 2015.

[22] C. V. RAMANA, R. J. SMITH, O. M. HUSSAIN and C. M. JULIEN, *Growth and surface characterization of V_2O_5 thin films made by pulsed-laser deposition*, Journal of Vacuum Science & Technology A **22**, pp. 2453–2458, 2004.

[23] D. O. KIKALOV, V.P. MALINENKO, A. L. PERGAMENT and G. B. STEFANOVICH, *Optical properties of thin films of amorphous vanadium oxides*, Technological Physics Letters **25**, pp. 331–333, 1999.

[24] S. LEE, T. L. MEYER, S. PARK, T. EGAMI and H.N. LEE, *Growth control of the oxidation state in vanadium oxide thin films*, Applied Physics Letters **105**, pp. 223115, 2014.

[25] E. UCHAKER, Y. Z. ZHENG, S. LI, S. L. CANDELARIA, S. HU and G. Z. CAO, *Better than crystalline: Amorphous vanadium oxide for sodium-ion batteries*, Journal of Materials Chemistry A **2**, pp. 18208–18214, 2014.

[26] X. SUN, C. ZHOU, M. XIE, T. HU, H. SUN, G. XIN, G. WANG, S. M. GEORGE and J. LIAN, *Amorphous vanadium oxide coating on graphene by atomic layer deposition for stable high energy lithium ion anodes*, Chemistry Communications **50**, pp. 10703–10706, 2014.

[27] K. LIU, S. LEE, S. YANG, O. DELAIRE and J. WU, *Recent progresses on physics and applications of vanadium dioxide*, Materials Today **21**, pp. 875–896, 2018.

[28] J.Y. KEMPF, B. SILVI, A. DIETRICH, C. R. A. CATLOW and B. MAIGRET, *Theoretical investigations of the electronic properties of vanadium oxides. 1. Pseudopotential periodic hartree-fock study of V_2O_5 crystal lattice*, Chemistry Materials **5**, pp. 641–647, 1993.

[29] V. EYERT and K. HÖCK, *Electronic structure of V_2O_5: Role of octahedral deformations*, Physical Review B **57**, pp. 12727–12737, 1998.

[30] A. CHAKRABARTI, K. HERMANN, R. DRUZINIC, M. WITKO, F. WAGNER and M. PETERSEN, *Geometric and electronic structure of vanadium pentoxide: a density functional bulk and surface study*, Physical Review B **59**, pp. 10583–10590, 1999.

[31] R. PLUGARU, I. MIHALACHE, C. ROMANITAN, F. COMANESCU, S. VULPE, G. CRACIUN, N.PLUGARU and N. DJOURELOV, *Light-Sensing Properties of Amorphous Vanadium Oxide Films Prepared by RF Sputtering*, Sensors **23**(4), pp. 1759, 2023.

[32] C. ROMANITAN, I. MIHALACHE, S. VULPE, M. STOIAN, I. V. TUDOSE, K. MOURATIS, O. TUTUNARU, N. DJOURELOV and M. SUCHEA, *Vanadium oxide by radio frequency magnetron sputtering and spray pyrolysis technique: structural and optical properties*, Proceedings of 2022 International Semiconductor Conference, Poiana Brasov, Romania, pp. 55–58, 2022.

[33] C. ROMANITAN, I. V. TUDOSE, K. MOURATIS, M. POPESCU, C. PACHIU, S. COURIS, E. KOUDOUMAS and M. P. SUCHEA, *Structural investigations in electrochromic vanadium pentoxide thin films*, Physica Status Solidi A **219**, pp. 2100431, 2022.

[34] K. MOURATIS, I.V. TUDOSE, A. BOURANTA, C. PACHIU, C. ROMANITAN, O. TUTUNARU, S. COURIS and E. KOUDOUMAS, *Annealing effect on the properties of electrochromic V 2 O 5 thin films grown by spray deposition technique*, Nanomaterials **10**, pp. 2397, 2020.

[35] D. BARRECA, L. ARMELAO, F. CACCAVALE, V. DI NOTO, A. GREGORI, G. A. RIZZI and E. TONDELLO, *Highly oriented V_2O_5 nanocrystalline thin films by plasma-enhanced chemical vapor deposition*, Chemistry Materials **12**, pp. 98–103, 2000.

[36] M. LOSURDO, D. BARRECA, G. BRUNO and E. TONDELLO, *Spectroscopic ellipsometry investigation of V_2O_5 nanocrystalline thin films*, Thin Solid Films 384, pp. 58–64, 2001.

[37] V. K. PECHARSKY and P. Y. ZAVALIJ, *Fundamentals of powder diffraction and structural characterization of materials*, 2nd edition, Springer, New York, 2009.

[38] M. BIRKHOLZ, P. F. FEWSTER and C. GENZEL, *Thin Film Analysis by X-Ray Scattering*, Wiley, Weinheim, 2006.

[39] L. J. MENG, R. A. SILVA, H. N. CUI, V. TEIXEIRA, M. P. DOS SANTOS and Z. XU, *Optical and structural properties of vanadium pentoxide films prepared by d.c. reactive magnetron sputtering*, Thin Solid Films **515**, pp. 195–200. 2006.

[40] M. KANG, S.W. KIM, Y. HWANG, Y. UM and J. W. RYU, *Temperature dependence of the interband transition in a V_2O_5 film*, AIP Advances **3**, pp. 052129, 2013.

[41] J. MEYER, K. ZILBERBERG, T. RIEDL and A. KAHN, *Electronic structure of Vanadium pentoxide: An efficient hole injector for organic electronic materials*, Journal of Applied Physics **110**, pp. 033710, 2011.

[42] A. BALTAKESMEZ, C. AYKA and B. GÜZELDIR, *Phase transition and changing properties of nanostructured V_2O_5 thin films deposited by spray pyrolysis technique, as a function of tungsten dopant*, Applied Physics A **125**, pp. 441, 2019.

[43] R. IRANI, S. M. ROZATI and S. BEKE, *Structural and optical properties of nanostructural V_2O_5 thin films deposited by spray pyrolysis technique: Effect of the substrate temperature*, Materials Chemistry and Physics **139**, pp. 489–493, 2013.

[44] Y. VIJAYAKUMAR, P. NAGARAJU, T. SREEKANTH, U. RUSHIDHAR and P.S. REDDY, *Effect of precursor volume on chemically sprayed V_2O_5 thin films for acetaldehyde detection*, Superlattices and Microstructures **153**, pp. 106870, 2021.

[45] M. MOUSAVI, A. KOMPANY, N. SHAHTAHMASEBI and M. M. BAGHERI-MOHAGHEGHI, *Study of structural, electrical and optical properties of vanadium oxide condensed films deposited by spray pyrolysis technique*, Advanced Manufacturing **1**, pp. 320–328, 2013.

[46] I. K. SALMAN, N. K. HASSAN and M. K. KHALAF, *The Influence of RF power, pressure and substrate temperature on optical properties of RF Sputtered vanadium pentoxide thin films*, Iraqi Journal of Physics **16**, pp. 42–47, 2019.

[47] D. PORWAL, A. C. M. ESTHER, I. N. REDDY, N. SRIDHARA, N. P. YADAV, D. RANGAPPA, P. BERA, C. ANANDAN, A. K. SHARMA and A. DEY, *Study of the structural, thermal, optical, electrical and nanomechanical properties of sputtered vanadium oxide smart thin films*, RSC Advanced **5**, pp. 35737–35745, 2015.

[48] C. R. AITA, Y. L. LIU, M.L. KAO and S. D. HANSEN, *Optical behavior of sputter-deposited vanadium pentoxide*, Journal of Applied Physics **60**, pp. 749–753, 1986.

[49] J.P. MEYN, T. DANGER, K. PETERMANN and G. HUBER, *Spectroscopic characterization of V4+ -doped Al2O3 and YAlO3*, Journal of Luminescence **55**, pp. 55–62, 1993.

[50] N. ÖZER, *Electrochemical properties of sol-gel deposited vanadium pentoxide films*, Thin Solid Films 305 pp. 80–87, 1997.

[51] G. SILVERSMIT, H. POELMAN and R. DE GRYSE, *Influence of magnetron deposition parameters on the stoichiometry of sputtered V_2O_5 films*, Surface and Interface Analysis **36**, pp. 1163–1166, 2004.

[52] J. MENDIALDUA, R. CASANOVA and Y. BARBAUX, *XPS studies of V_2O_5, V_6O_{13}, VO_2 and V_2O_3*, Journal of Electron Spectroscopy and Related Phenomena **71**, pp. 249–261, 1995.

[53] C. D. WAGNER, *Factors affecting quantitative determinations by X-ray photoelectron spectroscopy*, Analytical Chemistry **49**, pp. 12821290, 1977.